



CHORUS

This is the accepted manuscript made available via CHORUS. The article has been published as:

Effective electric-field force for a photon in a synthetic frequency lattice created in a waveguide modulator

Chengzhi Qin, Luqi Yuan, Bing Wang, Shanhui Fan, and Peixiang Lu

Phys. Rev. A **97**, 063838 — Published 18 June 2018

DOI: [10.1103/PhysRevA.97.063838](https://doi.org/10.1103/PhysRevA.97.063838)

Effective electric field force for photon in synthetic frequency lattice created in a waveguide modulator

Chengzhi Qin,¹ Luqi Yuan,² Bing Wang,^{1,*} Shanhui Fan,² and Peixiang Lu^{1,3,†}

¹School of Physics and Wuhan National Laboratory for Optoelectronics, Huazhong University of Science and Technology, Wuhan, 430074, China

²Department of Electrical Engineering, and Ginzton Laboratory, Stanford University, Stanford, California 94305, USA

³Laboratory for Optical Information Technology, Wuhan Institute of Technology, Wuhan, 430205, China

E-mails:

* wangbing@hust.edu.cn

† lupeixiang@hust.edu.cn

Abstract

Here we create an effective electric field force for photon in a synthetic frequency lattice to control the spectrum of light. The frequency lattice is created based on an optical waveguide modulator in which the dynamic index modulation can induce photonic transitions between adjacent lattice sites. We show that the wave vector mismatch during photonic transitions and periodic distribution of the modulation phase can be mapped into a linear-varying and a periodically-driven gauge potential, which gives rise to a constant and a harmonic oscillating force, respectively. Under different combinations of the constant and oscillating forces, we can realize the effects of frequency Bloch oscillations, anharmonic Bloch oscillations, Super-Bloch oscillations and directional frequency shift. With an appropriate choice of the magnitude of the oscillating force, we also achieve dynamic localization in the frequency domain. The realization of effective force provides a new mechanism to control the spectrum of light, which may find applications in frequency perfect imaging, efficient shifting and precise transduction.

I. INTRODUCTION

Photon is a neutral particle that does not couple to an external applied electric or magnetic field. Nevertheless, there has been significant recent works seeking to synthesize an effective electric and magnetic field that couple to photons [1-12]. In particular, an effective electric field for photons in real space can be achieved either by introducing photonic scalar potential in gradient-index or curved waveguide arrays [8-11], or through photonic gauge potential by controlling the modulation phases in dynamically modulated systems [12]. Moreover, there are also recent efforts to create effective electric field in the synthetic frequency dimension, by considering either a single or an array of micro-ring resonators undergoing dynamic modulations [13-15]. In these dynamically modulated micro-ring resonators, the effective force in frequency dimension is induced by the frequency detuning between the modulation frequency and the frequency spacing of adjacent resonant modes. This effective force can lead to Bloch oscillations in the frequency domain [14, 16-19], which provides a new capability to control the spectrum of light. However, in practice, the scheme in [14, 16] requires ring resonator structure with high quality factors in order to ensure that frequency conversion can occur in the duration of cavity lifetime.

In this work, we propose an alternative mechanism to achieve an effective electric field force in a synthetic frequency dimension by using a waveguide modulator structure. The structure consists of a phase modulator in a waveguide with a travelling wave modulation profile. The modulation can induce photonic transitions between different guided modes in the same photonic band, and thus creating a synthetic frequency dimension. We show that a constant force can arise, due to the mismatch between the modulation wave vector and the wave vector difference of adjacent modes going through a photonic transition. A harmonic oscillating force can also emerge as the modulation phase exhibits a periodic distribution in the propagation direction. With precise designs of the constant and oscillating force, we can realize the effects of frequency Bloch oscillations (BOs), anharmonic Bloch oscillations (ABOs) [20-22], Super-Bloch oscillations (SBOs) [23-27] and directional shift [28, 29]. By choosing specific magnitudes for the oscillating force, both frequency SBOs and directional shift can be completely suppressed, giving rise to the effect of frequency dynamic localization [9-12, 30, 31]. Compared to the temporal evolution of frequencies in ring resonators, the frequencies in the waveguide structure evolve in space rather than in time. So all the

effects could be more readily to observe since high-quality factor resonator is not required. Moreover, as the waveguide structure does not rely on the precisely designed resonances, the force here can be applied to arbitrarily input spectra, including both discrete and continuous ones.

II. THE MAIN RESULTS

A. Effective electric field force in synthetic frequency lattice

We start by considering the synthetic frequency lattice created in an optical waveguide modulator, as shown in Fig. 1(a). Differing from traditional travelling-wave phase modulator with two uniform strip electrodes [32-34], the phase modulator here consists an electrode array, such that the spatial distribution of the index modulation phase can be arbitrarily controlled. The instantaneous refractive index is thus $n(z, t) = n_0 + \Delta n \cdot \cos[\Omega t - q_m z + \phi(z)]$, where n_0 is the background index, Δn , q_m and $\phi(z)$ are the amplitude, wave vector and phase spatial distribution of the modulation profile, respectively. As shown schematically in Fig. 1(b), the modulation can create a discrete frequency lattice with a lattice constant Ω , giving rise to the photonic intraband transitions between adjacent guided modes with frequency $\omega_n = \omega_0 + n\Omega$ and wave vectors $\beta_n = \beta_0 + nq$ ($n = 0, \pm 1, \pm 2, \dots$). Here the wave vector mismatch is denoted by $\Delta q = q - q_m$. $a_n(z)$ represents the amplitude of n th-order mode, which is governed by the coupled-mode equation (see appendix A)

$$i \frac{\partial a_n(z)}{\partial z} = C \left(e^{i[\phi(z) + \Delta q \cdot z]} a_{n-1}(z) + e^{-i[\phi(z) + \Delta q \cdot z]} a_{n+1}(z) \right), \quad (1)$$

where $C = \Delta n k_0 / 2$ denotes the coupling strength between adjacent modes and k_0 is the vacuum wave number. It shows in Eq. (1) that there exists a nonreciprocal, z -dependent phase shift of $\phi(z) + \Delta q \cdot z$ accompanying photonic transitions, which flips the sign as the transition direction is reversed. This nonreciprocal phase shift is a photonic analogue of Peierls phase [1-3, 35-40], which can be mapped into a time-varying gauge potential and is responsible for the effective force in the frequency lattice.

Similar to spatial lattice, the lattice in frequency space as described by Eq. (1) can also support Bloch modes. The eigen Bloch mode in frequency lattice is an infinite width frequency comb $a_n(z) = a_0 \exp(in\phi_0) \exp(ik_z z)$, where a_0 is the amplitude and k_z is the collective propagation constant along z direction. $\phi_0 = k_\omega(0)\Omega$ with $k_\omega(0)$ being the initial Bloch wave vector along the frequency dimension. Substituting $a_n(z)$ into Eq. (1), we can obtain the z -dependent band structure for the frequency comb

$$k_z[k_\omega(z)] = -2C \cos[k_\omega(z)\Omega], \quad (2)$$

with the z -dependent Bloch wave vector given by

$$k_\omega(z) = k_\omega(0) - \frac{\phi(z) + \Delta q \cdot z}{\Omega}, \quad (3)$$

In the waveguide system, the propagation coordinate z acts as “time” t [41] with $z = ct$, where c is light speed in the waveguide. By choosing $c = 1$ for photons [42], the z -dependent Bloch momentum is thus equivalent to a time-dependent Bloch momentum $k_\omega(t)\Omega = \phi_0 - \phi(t) - \Delta q \cdot t$. Analogous to the situation where an electron experiences a momentum shift by interacting with an external applied vector potential [42, 43], here the shift of Bloch momentum indicates the presence of an effective gauge potential $A_{eff}(t) = \phi(t) + \Delta q \cdot t$ applied in the frequency lattice. This time-varying gauge potential corresponds to an effective electric field force of $F_{eff}(t) = -\partial A_{eff}(t)/\partial t = -\Delta q - \partial\phi(t)/\partial t$ [44, 45], or equivalently a z -dependent effective force

$$F_{eff}(z) = -\Delta q - \frac{\partial\phi(z)}{\partial z}, \quad (4)$$

The force consists of a constant and a z -dependent component, which are induced by the wave vector mismatch during photonic transitions and the spatial distribution of modulation phase, respectively. Due to the enormous degrees of freedom in choosing the format of the force, we can thus realize versatile transport dynamics in the frequency lattice. Specifically, with a periodic distribution for the modulation phase, the force can possess both dc and ac driving components. In the following, we will present several effects such as frequency BOs, ABOs, SBOs, directional shift and dynamic localization, which are realized under different combinations of the dc and ac driving forces.

B. Periodically oscillatory motions in the frequency lattice

One intriguing phenomenon in lattice structure exposed to external electric field is Bloch oscillation, which can be realized by applying a constant electric field force along the lattice structure. Here, we can realize frequency-space Bloch oscillations by applying only a constant force in the frequency lattice. This can be achieved by choosing a uniform phase distribution $\phi(z) = \phi$ such that $F_{dc} = -\Delta q$. Consider a finite-width frequency comb input with an initial Bloch momentum ϕ_0 , the frequency-

space group velocity is periodic, which is given by $v_{g,\omega}(z) = -\partial k_z[k_\omega(z)]/\partial k_\omega(z) = 2C\Omega\sin(\phi - \phi_0 + \Delta qz)$. The frequency shift is thus $\Delta\omega(z) = \int_0^z v_{g,\omega}(z')dz'$, with the center-of-mass trajectory described by

$$\Delta\omega(z) = \frac{2C\Omega}{\Delta q}[\cos(\phi - \phi_0) - \cos(\Delta qz + \phi - \phi_0)], \quad (5)$$

The envelope of the frequency comb experiences a cosine trajectory in the ω - z plane, manifesting the typical characterizations of Bloch oscillations. The corresponding oscillation period is $Z_B = 2\pi/|\Delta q|$, which is inversely proportional to the magnitude of the applied force. The oscillation amplitude is $2C\Omega/|\Delta q|$, indicating that the frequency shift is limited to $|\Delta\omega|_{\max} = 4C\Omega/|\Delta q|$ in the whole oscillation process. Moreover, the frequency shift direction can be controlled either by initial phase difference $\phi - \phi_0$ or the direction of applied force through changing the sign of the mismatched wave vector. In particular, under the wave vector matching condition as $\Delta q = 0$, the effective force will vanish, and hence there is no longer any oscillation.

It is straightforward to extend frequency BOs to other kinds of oscillatory motions through the superposition of constant forces. As a representative example, we consider the effect of frequency anharmonic Bloch oscillations (ABOs) [20-22], which can be realized by superimposing two commensurate constant forces in the frequency lattice. To achieve this goal, we adopt two commensurate sinusoidal modulation waves in the waveguide modulator

$$n(z, t) = n_0 + \Delta n_1 \cos(\Omega t - q_m z + \phi_1) + \Delta n_l \cos(l\Omega t - lq_m z + \phi_l), \quad (6)$$

where $\Omega, l\Omega$ are the frequencies of the fundamental and l -th modulation waves, which correspond to the wave numbers of q_m and lq_m for the two modulation waves, respectively. Here l is an arbitrarily chosen integer. $\Delta n_1, \Delta n_l, \phi_1, \phi_l$ are the respective modulation amplitudes and initial phases. The two modulation waves can induce respectively the nearest-neighbour and l -th order long-rang couplings in the frequency lattice, contributing simultaneously to the frequency evolution (see appendix B)

$$\Delta\omega(z) = \frac{2C_1\Omega}{\Delta q}[\cos(\phi_1 - \phi_0) - \cos(\Delta qz + \phi_1 - \phi_0)] + \frac{2C_l\Omega}{\Delta q}[\cos(\phi_l - l\phi_0) - \cos(l\Delta qz + \phi_l - l\phi_0)], \quad (7)$$

where $C_1 = \Delta n_1\beta_0/2n_0$ and $C_l = \Delta n_l\beta_0/2n_0$. The period of frequency ABOs is the same with frequency BOs, which equals to $Z_B = 2\pi/|\Delta q|$. It shows in Eq. (7) that the frequency ABOs can be regarded as the superposition of two independent frequency BOs driven by two commensurate constant forces of $F_1 = -\Delta q$ and $F_l = -l\Delta q$. The total frequency conversion direction is thus determined by the two

modulation phases and directions of the two forces.

In parallel with the frequency-space BOs and ABOs, frequency-space Super-Bloch oscillations (SBOs) can also be achieved by superimposing a constant and a harmonic oscillating force in the frequency lattice. Consider only one modulation wave with the modulation phase exhibiting a cosine spatial distribution $\phi(z) = \phi + \Delta\phi_m \cos(Q_m z + \phi_m)$, where ϕ , $\Delta\phi_m$, Q_m and ϕ_m are the background, amplitude, wave vector and initial phase of the modulation phase spatial distribution, respectively. The z -dependent effective force is thus $F_{\text{eff}}(z) = -\Delta q + Q_m \Delta\phi_m \sin(Q_m z + \phi_m)$. Since SBOs stem from the beat between BOs and the ac driving force [23-27], the mismatched wave vector Δq should be slightly detuned from the integer multiples of Q_m , that is $\Delta q = mQ_m + \Delta Q$. Here m is an integer and ΔQ is the detuned wave vector. The z -dependent group velocity in the frequency lattice is thus

$$v_{g,\omega}(z) = 2C\Omega \sin[\phi - \phi_0 + (mQ_m + \Delta Q)z + \Delta\phi_m \cos(Q_m z + \phi_m)], \quad (8)$$

Usually for very slight wave vector detune $\Delta Q \ll Q_m$, the term “ $\Delta Q z$ ” is slowly varying and can be considered as constant in an ac driving period of $2\pi/Q_m$. So the average periodic group velocity in an driving period reads (see appendix B)

$$\langle v_{g,\omega}(z) \rangle = 2C\Omega J_m(\Delta\phi_m) \sin[\Delta Q z + \phi - \phi_0 + m(\frac{\pi}{2} - \phi_m)], \quad (9)$$

where J_m is the m th-order Bessel function. The average center trajectory of the frequency comb is

$$\langle \Delta\omega(z) \rangle = \frac{2C\Omega J_m(\Delta\phi_m)}{\Delta Q} \left\{ \cos[\phi - \phi_0 + m(\frac{\pi}{2} - \phi_m)] - \cos[\Delta Q z + \phi - \phi_0 + m(\frac{\pi}{2} - \phi_m)] \right\}, \quad (10)$$

So the frequency comb also experiences a cosine trajectory in the ω - z plane. The period of frequency SBOs is $Z_{\text{SB}} = 2\pi/|\Delta Q|$, which is inversely proportional to the detuned wave vector ΔQ . Compared to BOs, the oscillation amplitude and period of SBOs are enlarged by $J_m(\Delta\phi_m)\Delta q/\Delta Q$ and $\Delta q/\Delta Q$ times, respectively. Similarly, as the detuned wave vector vanishes with $\Delta Q = 0$, the period of SBOs will become infinity, the oscillation breaks down, even though both the dc and ac forces still exist.

All the theoretical analysis above can be verified by numerical simulations of the frequency evolutions. The results are shown in Fig. 2 which are obtained by solving the coupled-mode equation of Eq. (1). In the simulations, we choose a slab waveguide with background dielectric constant $\epsilon_d = 4.58$ ($n_0 = 2.14$) and thickness $d = 0.5 \mu\text{m}$. The modulation amplitude and frequency are $\Delta\epsilon = 5 \times 10^{-3}$ and $\Omega/2\pi = 20 \text{ GHz}$, both of which are attainable with state-of-the art experimental techniques

[33, 46, 47]. The central input optical wavelength is chosen as the telecommunication wavelength $\lambda_0 = 1.55 \mu\text{m}$ and the modulation wave wavenumber is $q_m = 2q$. So the wave vector mismatch is $|\Delta q| = |q - q_m| = 0.93 \text{ mm}^{-1}$, corresponding to a Bloch oscillation period $Z_B = 2\pi/|\Delta q| \sim 6.76 \text{ mm}$. Figure 2(a) shows the spectral evolutions of BOs for a finite-width frequency comb input $a_n(0) = a_0 \exp[-(n\Omega/W)^2] \exp(in\phi_0)$, where W and ϕ_0 are the width of the Gaussian envelope and initial Bloch momentum, respectively. By choosing $W = 5\Omega$ and $\phi - \phi_0 = \pi/2$, the frequency comb exhibits a cosine trajectory in ω - z plane, which agrees perfectly with the theoretical prediction of Eq. (4) (also denoted by the red solid line, same below). Interestingly, under a single frequency input, as shown in Fig. 2(b), the spectrum evolution manifests a breathing pattern and exhibits “self-focusing” at integer multiples of Bloch period Z_B . This can be interpreted in terms of Fourier analysis. A single frequency can be regarded as the superposition of all Bloch-mode frequency combs over the entire Brillouin zone. With all frequency combs sharing the same oscillation period, there will exist nodes at integer multiples of Z_B , leading to the emergence of “frequency self-focusing”.

Figures 2(c) and 2(d) show the dynamics of frequency ABOs under a frequency comb and a single frequency input, respectively. In the simulations, we choose $l = 2$ such that both the nearest- and next-nearest couplings are induced in the frequency lattice. The spectral evolutions of ABOs are thus the interference pattern of two sets of BOs. For a frequency comb input shown in Fig. 2(c), we choose $W = 8\Omega$, equal coupling strengths $C_1 = C_2$ and same modulation phases $\phi_1 - \phi_0 = \phi_2 - \phi_0 = \pi$, the spectral evolution can thus trace out the superposition of two cosine trajectories. For a single frequency input, as shown in Fig. 2(d), the spectral evolution also exhibits a breathing pattern, but with a waist emerging at half oscillation period of Z_B . Again, the spectrum also manifests the effect of “self-focusing” at integer multiples of Z_B . Figures 2(e) and 2(d) show the dynamics of frequency SBOs under a frequency comb and a single frequency input, which manifest an enlarged cosine trajectory and breathing pattern, respectively. By choosing $W = 50\Omega$, $\Delta\phi_m = \pi/2$, $\phi - \phi_0 = \phi_m - \phi_0 = 0$ and $\Delta Q = \Delta q/20$, we have $Z_{SB} = 20Z_B$, the SBOs period is enlarged by 20 times compared to that of BOs. Similar to BOs, frequency SBOs can also exhibit “frequency self-focusing” at integer multiples of Z_{SB} , which can be flexibly controlled by varying the detuned wave vector. Generally, any periodic oscillatory motions can realize frequency self-imaging for arbitrarily input spectra due to their periodic revival nature. In appendix C, we simulate the self-imaging processes for both discrete and continuous spectra, all of which agree well with the theoretical predictions. It should be mentioned

that the spectral imaging process is perfect without any resolution limitation since it relies on the periodically oscillatory motions. This is different from the spatial imaging process for which the resolution is basically constrained by the diffraction limit [48, 49]. As such, the frequency perfect imaging can find applications in signal reshaping and spectral reconstructions for both optical communication and signal processing.

C. Directional transport and dynamic localization in the frequency lattice

In contrast to the above periodically oscillatory motions of frequency BOs, ABOs and SBOs, directional transport is another typical form of motion in which the wave packet can extend across the whole lattice [28, 29]. To realize frequency directional transport, we can remove the dc force with $\Delta q = 0$ and apply only the ac force $F_{ac}(z) = Q_m \Delta \phi_m \sin(Q_m z + \phi_m)$. In one ac driving period of $2\pi/Q_m$, the input frequency comb exhibits a constant average group velocity $\langle v_{g,\omega} \rangle = 2C\Omega J_0(\Delta \phi_m) \sin(\phi - \phi_0)$ in the frequency lattice, corresponding to a directional frequency shift (see appendix B)

$$\langle \Delta \omega(z) \rangle = 2C\Omega J_0(\Delta \phi_m) \sin(\phi - \phi_0) z, \quad (11)$$

where J_0 is zeroth-order Bessel function. As the ac force vanishes with $\Delta \phi_m = 0$, we have $\Delta \omega(z) = 2C\Omega \sin(\phi - \phi_0) z$, the spectral evolution will degrade into the force-free discrete diffraction of a Bloch mode in the waveguide array [33, 50-52]. So the effect of ac force is the renormalization of coupling coefficient, with C replaced by $J_0(\Delta \phi_m) C$. The corresponding frequency shift is also renormalized by the multiplicative factor of $J_0(\Delta \phi_m)$. As the ac force $\Delta \phi_m$ is fixed, the direction of frequency shift can be continuously tuned by the phase difference $\phi - \phi_0$, as shown in Fig. 3(a). Particularly for $\phi - \phi_0 = 0$ or π shown in Fig. 3(b), the spectral shift will vanish. While for $\phi - \phi_0 = \pm \pi/2$ shown in Figs. 3(c) and 3(d), the frequency comb experiences maximum blue and red shifts. For a single frequency input, as shown in Fig. 3(d), the frequency manifests a linear diffraction with a cone-like pattern. Since a single frequency input represents the excitation of all Bloch modes in the entire Brillouin zone, all directions of frequency diffraction will emerge. The boundary of the cone-like pattern is determined by the maximum red and blue shifts for frequency combs with $\phi - \phi_0 = \pm \pi/2$. Specifically, the cone-like pattern can be equivalently described by the average amplitude spectrum

$$|\langle a_n(z) \rangle| = a_0 |J_n[2CJ_0(\Delta \phi_m) z]|, \quad (12)$$

The original and equivalent average amplitude spectra evolutions for a single frequency input are

shown in Figs. 3(e) and 3(f), which can agree well with each other. Particularly for a vanished ac force $\Delta\phi_m = 0$, we have $|\langle a_n(z) \rangle| = a_0 |J_n(2Cz)|$, the frequency evolution will also degrade into the force-free discrete diffraction pattern for a single site excitation in the waveguide arrays [33, 50-52].

In particular, both frequency SBOs and directional shift can be completely suppressed with an appropriate choice of the magnitude of the ac force. For frequency directional shift shown in Fig. 4, the maximum frequency shift in an ac driving period follows the 0th-order Bessel function of $\Delta\phi_m$. As $\Delta\phi_m$ is chosen as the zeroes of J_0 function, as indicated in Eq. (11), the spectral shift for each frequency comb vanishes, giving rise to the effect of frequency dynamic localization. In inserted Fig. 4(a), we input a single frequency and choose $\Delta\phi_m = 2.40483$ (first zero of J_0), the frequency manifests complete suppression of diffraction in the propagation process. For frequency SBOs as denoted in Eq. (10), when $\Delta\phi_m$ is chosen as the zeroes of m th-order Bessel function, the oscillation amplitude of SBOs will also become zero. The maximum frequency shift of SBOs for different $\Delta\phi_m$ is shown by the blue curve in Fig. 4 where we choose $m = 1$. In the inserted Fig. 4(b), we choose the first zero of J_1 with $\Delta\phi_m = 3.83171$ and input a single frequency, the oscillation is completely suppressed, which can also lead to the effect of frequency dynamic localization.

III. CONCLUSIONS

In summary, we realize an effective electric field force for photon in a frequency lattice created with a periodically-driven waveguide modulator. The force contains a constant and a harmonic oscillating component, with which we realize the effects of frequency BOs, ABOs, SBOs, directional shifting, and dynamic localization. All the effects can provide new capabilities to precisely and efficiently control the spectrum of light. Frequency BOs, ABOs, and SBOs can be used in frequency perfect imaging for arbitrarily input spectra while frequency directional shift and dynamic localization may find applications in precise spectral shifting and transduction. Finally, due to the universality of synthetic electric field, all the effects demonstrated here can be readily generalized to other classical wave systems, enabling the precise spectral control for acoustic, mechanical and matter waves.

ACKNOWLEDGMENTS

The work is supported by the 973 Program (No. 2014CB921301), the National Natural Science

Foundation of China (No. 11674117) and Graduates' Innovation Fund, Huazhong University of Science and Technology (No. 5003012009). L. Y and S. F. in addition acknowledge the support for the U. S. National Science Foundation Grant No. CBET-1641069.

APPENDIX A: COUPLED-MODE EQUATION IN THE FREQUENCY LATTICE

In appendix A, we derive the coupled-mode equation in the frequency lattice. For the waveguide modulator driven by a sinusoidal RF signal, the instantaneous refractive index is given by

$$n(z, t) = n_0 + \Delta n \cdot \cos[\Omega t - q_m z + \phi(z)], \quad (\text{A1})$$

Here we assume the modulation is uniform in the transverse direction. The instantaneous dielectric modulation thus reads

$$\varepsilon(z, t) = \varepsilon_d + \Delta\varepsilon \cdot \cos[\Omega t - q_m z + \phi(z)], \quad (\text{A2})$$

where $\varepsilon_d = n_0^2$, $\Delta\varepsilon = 2n_0\Delta n$. The quadratic term Δn^2 is neglected here since $\Delta n \ll n_0$. The modulation can create a frequency lattice in the TE₀ band, with the electric field distribution given by

$$E(x, z, t) = \sum_n a_n(z) \psi_n(x) e^{i(\omega_n t - \beta_n z)}, \quad (\text{A3})$$

where $\omega_n = \omega_0 + n\Omega$ and $\beta_n = \beta_0 + nq$ ($n = 0, \pm 1, \pm 2, \dots$) are the frequency and propagation constant of n th-order TE₀ mode. $\psi_n(x)$ is the transverse mode profile. The electric field distribution satisfies

$$\nabla^2 E(x, z, t) - \frac{1}{c^2} \frac{\partial^2}{\partial t^2} [\varepsilon(z, t) E(x, z, t)] = 0, \quad (\text{A4})$$

Substituting Eqs. (A2) and (A3) into (A4), we can obtain

$$\left(\frac{\partial^2}{\partial x^2} + \frac{\partial^2}{\partial z^2} \right) E(x, z, t) - \frac{\varepsilon_d}{c^2} \frac{\partial^2}{\partial t^2} E(x, z, t) = \frac{\Delta\varepsilon}{c^2} \frac{\partial^2}{\partial t^2} \{ \cos[\Omega t - q_m z + \phi(z)] E(x, z, t) \}, \quad (\text{A5})$$

By applying the slowly varying amplitude approximation, the left side of Eq. (A5) is

$$-\sum_n 2i\beta_n \frac{\partial a_n(z)}{\partial z} \psi_n(x) e^{i(\omega_n t - \beta_n z)}, \quad (\text{A6})$$

By denoting $\omega_n \pm \Omega = \omega_{n\pm 1}$, $\beta_n \pm q = \beta_{n\pm 1}$, the right side of Eq. (A5) is

$$\begin{aligned}
& \frac{\partial^2}{\partial t^2} \left\{ \frac{1}{2} \left(e^{i[\Omega t - q_m z + \phi(z)]} + e^{-i[\Omega t - q_m z + \phi(z)]} \right) \sum_n a_n(z) \psi_n(x) e^{i(\omega_n t - \beta_n z)} \right\} \\
&= \frac{1}{2} \frac{\partial^2}{\partial t^2} \sum_n a_n(z) \psi_n(x) \left(e^{i(\omega_n + \Omega)t} e^{-i(\beta_n + q_m)z} e^{i\phi(z)} + e^{i(\omega_n - \Omega)t} e^{-i(\beta_n - q_m)z} e^{-i\phi(z)} \right) \\
&= -\frac{1}{2} \sum_n a_n(z) \psi_n(x) \left(\omega_{n+1}^2 e^{i(\omega_{n+1} t - \beta_{n+1} z)} e^{i[\phi(z) + \Delta q \cdot z]} + \omega_{n-1}^2 e^{i(\omega_{n-1} t - \beta_{n-1} z)} e^{-i[\phi(z) + \Delta q \cdot z]} \right),
\end{aligned} \tag{A7}$$

where $\Delta q = q - q_m$ is the mismatched wave vector. By substituting $(n \pm 1)$ by n , we have

$$\sum_n a_n(z) \psi_n(x) \omega_{n \pm 1}^2 e^{i(\omega_{n \pm 1} t - \beta_{n \pm 1} z)} = \sum_n a_{n \pm 1}(z) \psi_{n \pm 1}(x) \omega_n^2 e^{i(\omega_n t - \beta_n z)}, \tag{A8}$$

Since $\Omega \ll \omega_0$, the mode profiles satisfy $\psi_{n \pm 1}(x) \approx \psi_n(x)$, we can obtain the coupled-mode equation

$$i \frac{\partial a_n(z)}{\partial z} = C_n \left(e^{i[\phi(z) + \Delta q \cdot z]} a_{n-1}(z) + e^{-i[\phi(z) + \Delta q \cdot z]} a_{n+1}(z) \right), \tag{A9}$$

where the coupling strength between the n th and $(n \pm 1)$ th-order mode is given by

$$C_n = \frac{\Delta \varepsilon \cdot \omega_n^2}{4 \beta_n c^2} = \frac{\Delta n \beta_0}{2 n_0}, \tag{A10}$$

Since $\Omega \ll \omega_0$, we can neglect the dispersion of coupling strength and denote $C_n = C$. To solve the coupled-mode equation of Eq. (A9), we can truncate the order to the maximum $n = M$. By demoting $|\varphi(z)\rangle = [a_1(z), a_2(z), \dots, a_M(z)]^T$ with $N = 2M + 1$, we can thus cast the coupled-mode equation into a time-dependent Schrödinger equation

$$i \frac{\partial |\varphi(z)\rangle}{\partial z} = \mathbf{H}(z) |\varphi(z)\rangle, \tag{A11}$$

where the z -dependent matrix $\mathbf{H}(z)$ is given by

$$\mathbf{H}(z) = \begin{pmatrix} 0 & C e^{-i[\phi(z) + \Delta q \cdot z]} & 0 & \dots & 0 & 0 \\ C e^{i[\phi(z) + \Delta q \cdot z]} & 0 & C e^{-i[\phi(z) + \Delta q \cdot z]} & \dots & 0 & 0 \\ 0 & C e^{i[\phi(z) + \Delta q \cdot z]} & 0 & \dots & 0 & 0 \\ \vdots & \vdots & \vdots & \ddots & \vdots & \vdots \\ 0 & 0 & 0 & \dots & 0 & C e^{-i[\phi(z) + \Delta q \cdot z]} \\ 0 & 0 & 0 & \dots & C e^{i[\phi(z) + \Delta q \cdot z]} & 0 \end{pmatrix}, \tag{A12}$$

The dynamics of frequency BOs, SBOs, directional shift and dynamic localization can be obtained by solving Eq. (A11) numerically.

APPENDIX B: FREQUENCY ABOS, SBOS, DIRECTIONAL SHIFT AND DYNAMICAL LOCALIZATION

To induce frequency ABOs, as demonstrated in the main text, there should exist two commensurate sinusoidal wave modulations

$$n(z, t) = n_0 + \Delta n_1 \cos(\Omega t - q_m z + \phi_1) + \Delta n_l \cos(l\Omega t - lq_m z + \phi_l), \quad (\text{B1})$$

with the corresponding coupled-mode equation given by

$$i \frac{\partial a_n(z)}{\partial z} = C_1 [e^{i(\phi_1 + \Delta q z)} a_{n-1}(z) + e^{-i(\phi_1 + \Delta q z)} a_{n+1}(z)] + C_l [e^{i(\phi_l + l\Delta q z)} a_{n-l}(z) + e^{-i(\phi_l + l\Delta q z)} a_{n+l}(z)], \quad (\text{B2})$$

The corresponding z -dependent band structure thus reads

$$k_z[k_\omega(z)] = -2C_1 \cos(k_\omega \Omega - \phi_1 - \Delta q z) - 2C_l \cos(lk_\omega \Omega - \phi_l - l\Delta q z), \quad (\text{B3})$$

with the z -dependent group velocity given by

$$v_{g,\omega}(z) = -2C_1 \Omega \sin(k_\omega \Omega - \phi_1 - \Delta q z) - 2C_l \Omega \sin(lk_\omega \Omega - \phi_l - l\Delta q z), \quad (\text{B4})$$

The corresponding frequency shift is

$$\Delta\omega(z) = \frac{2C_1 \Omega}{\Delta q} [\cos(\phi_1 - \phi_0) - \cos(\Delta q z + \phi_1 - \phi_0)] + \frac{2C_l \Omega}{\Delta q} [\cos(\phi_l - l\phi_0) - \cos(l\Delta q z + \phi_l - l\phi_0)], \quad (\text{B5})$$

Then we consider frequency SBOs, the z -dependent group velocity along frequency dimension is

$$\begin{aligned} v_{g,\omega}(z) &= 2C\Omega \sin[\phi - \phi_0 + (mQ_m + \Delta Q)z + \Delta\phi_m \cos(Q_m z + \phi_m)] \\ &= 2C\Omega \sin[(\phi - \phi_0 + \Delta Qz) + m(\frac{\pi}{2} - \phi_m) + m(Q_m z + \phi_m - \frac{\pi}{2}) - \Delta\phi_m \sin(Q_m z + \phi_m - \frac{\pi}{2})] \\ &= 2C\Omega \sin[(\phi - \phi_0 + \Delta Qz) + m(\frac{\pi}{2} - \phi_m)] \cos[\Delta\phi_m \sin(Q_m z + \phi_m - \frac{\pi}{2}) - m(Q_m z + \phi_m - \frac{\pi}{2})] \\ &\quad - 2C\Omega \cos[(\phi - \phi_0 + \Delta Qz) + m(\frac{\pi}{2} - \phi_m)] \sin[\Delta\phi_m \sin(Q_m z + \phi_m - \frac{\pi}{2}) - m(Q_m z + \phi_m - \frac{\pi}{2})], \end{aligned} \quad (\text{B6})$$

Since $\Delta Q \ll Q_m$, the term “ ΔQz ” is slowly varying and can be considered as constant in the period of $2\pi/Q_m$. By denoting $\theta = Q_m z + \phi_m - \pi/2$, we can obtain average group velocity in the frequency axis

$$\begin{aligned}
\langle v_{g,\omega}(z) \rangle &= \frac{Q_m}{2\pi} \int_0^{2\pi/Q_m} v_{g,\omega}(z') dz' \\
&= \frac{Q_m}{2\pi} 2C\Omega \sin[(\phi - \phi_0 + \Delta Qz) + m(\frac{\pi}{2} - \phi_m)] \int_0^{2\pi/Q_m} \cos[\Delta\phi_m \sin(Q_m z' + \phi_m - \frac{\pi}{2}) - m(Q_m z' + \phi_m - \frac{\pi}{2})] dz' \\
&\quad - \frac{Q_m}{2\pi} 2C\Omega \cos[(\phi - \phi_0 + \Delta Qz) + m(\frac{\pi}{2} - \phi_m)] \int_0^{2\pi/Q_m} \sin[\Delta\phi_m \sin(Q_m z' + \phi_m - \frac{\pi}{2}) - m(Q_m z' + \phi_m - \frac{\pi}{2})] dz' \\
&= \frac{1}{2\pi} 2C\Omega \sin[(\phi - \phi_0 + \Delta Qz) + m(\frac{\pi}{2} - \phi_m)] \int_{\phi_m - \frac{\pi}{2}}^{\phi_m + \frac{3\pi}{2}} \cos[\Delta\phi_m \sin(\theta) - m\theta] d\theta \\
&\quad - \frac{1}{2\pi} 2C\Omega \cos[(\phi - \phi_0 + \Delta Qz) + m(\frac{\pi}{2} - \phi_m)] \int_{\phi_m - \frac{\pi}{2}}^{\phi_m + \frac{3\pi}{2}} \sin[\Delta\phi_m \sin(\theta) - m\theta] d\theta \\
&= 2C\Omega J_m(\Delta\phi_m) \sin[\Delta Qz + \phi - \phi_0 + m(\frac{\pi}{2} - \phi_m)],
\end{aligned} \tag{B7}$$

Here we utilize the identities as follows. For arbitrary x , φ , the identities are

$$\begin{cases} \frac{1}{2\pi} \int_{\varphi}^{\varphi+2\pi} \cos[x \sin(\theta) - m\theta] d\theta = J_m(x), \\ \frac{1}{2\pi} \int_{\varphi}^{\varphi+2\pi} \sin[x \sin(\theta) - m\theta] d\theta = 0, \end{cases} \tag{B8}$$

The frequency shift is $\langle \Delta\omega(z) \rangle = \int_0^z \langle v_{g,\omega}(z') \rangle dz'$, leading to the frequency center trajectory

$$\langle \Delta\omega(z) \rangle = \frac{2C\Omega J_m(\Delta\phi_m)}{\Delta Q} \left\{ \cos[\phi - \phi_0 + m(\frac{\pi}{2} - \phi_m)] - \cos[\Delta Qz + \phi - \phi_0 + m(\frac{\pi}{2} - \phi_m)] \right\}, \tag{B9}$$

Next, we consider frequency directional shift with $\Delta q = 0$, the z -dependent average group velocity in a period of $2\pi/Q_m$ is given by

$$\begin{aligned}
\langle v_{g,\omega}(z) \rangle &= \frac{Q_m}{2\pi} \int_0^{2\pi/Q_m} 2C\Omega \sin[\phi - \phi_0 + \Delta\phi_m \cos(Q_m z' + \phi_m)] dz' \\
&= \frac{Q_m}{2\pi} 2C\Omega \int_0^{2\pi/Q_m} \left\{ \sin(\phi - \phi_0) \cos[\Delta\phi_m \cos(Q_m z' + \phi_m)] + \cos(\phi - \phi_0) \sin[\Delta\phi_m \cos(Q_m z' + \phi_m)] \right\} dz' \\
&= \frac{Q_m}{2\pi} 2C\Omega \sin(\phi - \phi_0) \int_0^{2\pi/Q_m} \left\{ J_0(\Delta\phi_m) + 2 \sum_{n=1}^{\infty} (-1)^n J_{2n}(\Delta\phi_m) \cos[2n(Q_m z' + \phi_m)] \right\} dz' \\
&\quad - \frac{Q_m}{2\pi} 2C\Omega \cos(\phi - \phi_0) \int_0^{2\pi/Q_m} \left\{ 2 \sum_{n=1}^{\infty} (-1)^n J_{2n-1}(\Delta\phi_m) \cos[2n(Q_m z' + \phi_m)] \right\} dz' \\
&= 2C\Omega J_0(\Delta\phi_m) \sin(\phi - \phi_0),
\end{aligned} \tag{B10}$$

So the center-of-mass of the frequency comb exhibits a line trajectory which is given by

$$\langle \Delta\omega(z) \rangle = 2C\Omega J_0(\Delta\phi_m) \sin(\phi - \phi_0) z, \tag{B11}$$

For a single frequency input with initial electric field distribution $E_{in}(t) = a_0 \exp(i\omega_0 t)$, the dynamic

index modulation imposes a time-varying phase factor on the optical mode, and the z -dependent instantaneous electric field is given by

$$E(z, t) = a_0 \exp(i\omega_0 t) \exp\{i2Cz \cos[\Omega t + \phi + \Delta\phi_m \cos(Q_m t + \phi_m)]\}, \quad (\text{B12})$$

So the average electric field distribution in a period of ac force $2\pi/Q_m$ is

$$\begin{aligned} \langle E(z, t) \rangle &= \frac{1}{T} \int_0^T E(z, t') dt' \\ &= a_0 \exp(i\omega_0 t) \exp[i2Cz J_0(\Delta\phi_m) \cos(\Omega t + \phi)] \\ &= a_0 \exp(i\omega_0 t) \sum_{n=-\infty}^{\infty} (i)^n J_n[2Cz J_0(\Delta\phi_m)] \exp[in(\Omega t + \phi)], \end{aligned} \quad (\text{B13})$$

By using Fourier analysis, we can obtain the average amplitude spectrum at coordinate z

$$|\langle a_n(z) \rangle| = a_0 |J_n[2CJ_0(\Delta\phi_m)z]|, \quad (\text{B14})$$

APPENDIX C: APPLICATIONS IN SPECTRAL PERFECT IMAGING

As demonstrated in the main text that BOs, ABOs and SBOs can all realize frequency self-focusing for a single frequency input. In appendix C, we exploit these effects to find applications in spectral perfect imaging. In principle, any oscillatory motion can be used for imaging applications due to the periodic revival nature. As particular examples, we choose frequency BOs, ABOs for demonstrations and input single frequency, frequency comb and continuous Gaussian spectra, respectively. We also perfect first-principle numerical simulations by using COMSOL Multiphysics to further verify these results. To save the computational time, we choose a high modulation frequency of $\Omega/2\pi = 4$ THz and large modulation amplitude of $\Delta\epsilon = 0.5$, both of which are different from those in the main text. It should be mentioned that different choices of modulation parameters have no influence on the physics underneath.

For discrete spectrum input, we firstly consider a single frequency and choose $L = Z_B$. As shown in Fig. 5(a), the single frequency is converted to a frequency comb in the first half period and recovers to a single frequency in the second half, thus manifesting the phenomenon of spectral self-imaging. In Fig. 5(b), the input frequency comb also experiences the perfect imaging after tracing out an entire cosine trajectory. Figures 5(c) to 5(d) show the frequency ABOs under a single frequency and a frequency comb input, both of which can exhibit spectral self-imaging effects. The

first-principle simulated and the theoretical spectra at $z = 0, Z_B/4, Z_B/2, 3Z_B/4$ and Z_B are incorporated in Fig. 5, which can agree well with each other.

For a continuous input spectrum, we choose an ultra-short pulse with a Gaussian envelope

$$a(x, t) = A \psi_0(x) \cos(\omega_0 t) e^{-\frac{(t-t_0)^2}{\Delta t}}, \quad (\text{C1})$$

where A and $\psi_0(x)$ are the amplitude and transverse profile of the TE_0 mode at the carrier wave frequency ω_0 . t_0 and Δt are the time delay and width of the Gaussian pulse, respectively. The ultra-short Gaussian pulse has a spectrum of Gaussian shape, which is given by

$$\tilde{a}(\omega, z = 0) = A' e^{-\frac{(\omega-\omega_0)^2}{\Delta\omega}}, \quad (\text{C2})$$

where A' is a constant coefficient. The width of the Gaussian spectrum is thus

$$\Delta\omega = \frac{2}{\Delta t}, \quad (\text{C3})$$

The continuous spectral evolutions for frequency BOs are shown in Fig. 6. The modulation phase with respect to the pulse arrival time is $\phi = 0, \pi, -\pi/2, \pi/2$, for all of which the Gaussian spectra can be perfectly reconstructed by propagating one BOs period of Z_B . For $\phi = 0$ shown in Fig. 6(a), the Gaussian spectrum experiences a red shift and bandwidth expansion in the first half period and then a time-reversed process in the second half, ultimately restoring to the initial spectrum. While for $\phi = \pi$ shown in Fig. 6(b), the spectrum evolution is mirror symmetric with that for $\phi = 0$. For $\phi = -\pi/2$ and $\pi/2$, as shown in Figs. 6(c) and 6(d), the spectrum exhibits a red (blue) shift in the first half period and then a blue (red) shift in the second, both of which are perfectly reconstructed at $z = Z_B$. Actually, the effect of frequency self-imaging is independent of the format of the input spectrum, which can be applicable to any kind of input spectrum.

References

- [1] J. Dalibard, F. Gerbier, G. Juzeliūnas, and P. Öhberg, *Rev. Mod. Phys.* **83**, 1523 (2011).
- [2] K. Fang, Z. Yu, and S. Fan, *Phys. Rev. Lett.* **108**, 153901 (2012).
- [3] K. Fang, Z. Yu, and S. Fan, *Nat. Photonics* **6**, 782 (2012).
- [4] N. Schine, A. Ryou, A. Gromov, A. Sommer, and J. Simon, *Nature (London)* **534**, 671 (2016).
- [5] M. C. Rechtsman, J. M. Zeuner, A. Tünnermann, S. Nolte, M. Segev, and A. Szameit, *Nat. Photonics* **7**, 153 (2012).
- [6] G. L. Rikken and B. A. van Tiggelen, *Phys. Rev. Lett.* **108**, 230402 (2012).
- [7] I. Martin, G. Refael, and B. Halperin, *Phys. Rev. X* **7**, 041008 (2017).
- [8] G. Lenz, I. Talanina, and C. M. d. Sterke, *Phys. Rev. Lett.* **83**, 963 (1999).
- [9] F. Dreisow, A. Szameit, M. Heinrich, T. Pertsch, S. Nolte, A. Tünnermann, and S. Longhi, *Phys. Rev. Lett.* **102**, 076802 (2009).
- [10] A. Szameit, I. L. Garanovich, M. Heinrich, A. A. Sukhorukov, F. Dreisow, T. Pertsch, S. Nolte, A. Tünnermann, and Y. S. Kivshar, *Nat. Phys.* **5**, 271 (2009).
- [11] A. Szameit *et al.*, *Phys. Rev. Lett.* **104**, 223903 (2010).
- [12] L. Yuan and S. Fan, *Phys. Rev. Lett.* **114**, 243901 (2015).
- [13] L. Yuan, Y. Shi, and S. Fan, *Opt. Lett.* **41**, 741 (2016).
- [14] L. Yuan and S. Fan, *Optica* **3**, 1014 (2016).
- [15] T. Ozawa, H. M. Price, N. Goldman, O. Zilberberg, and I. Carusotto, *Phys. Rev. A* **93**, 043827 (2016).
- [16] S. Longhi, *Opt. Lett.* **30**, 786 (2005).
- [17] U. Peschel, C. Bersch, and G. Onishchukov, *Open Physics* **6**, 619 (2008).
- [18] C. Bersch, G. Onishchukov, and U. Peschel, *Opt. Lett.* **34**, 2372 (2009).
- [19] C. Bersch, G. Onishchukov, and U. Peschel, *Appl. Phys. B* **104**, 495 (2011).
- [20] G. Wang, J. P. Huang, and K. W. Yu, *Opt. Lett.* **35**, 1908 (2010).
- [21] F. Dreisow, G. Wang, M. Heinrich, S. Nolte, R. Keil, and A. Szameit, *Opt. Lett.* **36**, 3963 (2011).
- [22] J. Stockhofe and P. Schmelcher, *Phys. Rev. A* **91**, 023606 (2015).
- [23] E. Haller, R. Hart, M. J. Mark, J. G. Danzl, L. Reichsöllner, and H. C. Nägerl, *Phys. Rev. Lett.* **104**, 200403 (2010).

- [24] K. Kudo and T. S. Monteiro, [Phys. Rev. A **83**, 053627 \(2011\)](#).
- [25] S. Arlinghaus and M. Holthaus, [Phys. Rev. B **84**, 054301 \(2011\)](#).
- [26] E. Díaz, A. García Mena, K. Asakura, and C. Gaul, [Phys. Rev. A **87**, 015601 \(2013\)](#).
- [27] S. Longhi and G. Della Valle, [Phys. Rev. B **86**, 075143 \(2012\)](#).
- [28] S. Longhi, [Phys. Rev. B **80**, 235102 \(2009\)](#).
- [29] C. E. Creffield and F. Sols, [Phys. Rev. A **84**, 023630 \(2011\)](#).
- [30] D. H. Dunlap and V. M. Kenkre, [Phys. Rev. B **34**, 3625 \(1986\)](#).
- [31] M. Holthaus, [Phys. Rev. Lett. **69**, 351 \(1992\)](#).
- [32] W. S. Chang, *RF Photonic Technology in Optical Fiber Links* (Cambridge University Press, New York, 2002).
- [33] S. Wang, B. Wang, C. Qin, K. Wang, H. Long, and P. Lu, [Opt. Quant. Elec. **49**, 389 \(2017\)](#).
- [34] C. Qin, F. Zhou, Y. Peng, D. Sounas, X. Zhu, B. Wang, J. Dong, X. Zhang, A. Alù and P. Lu, [Phys. Rev. Lett. **120**, 133901 \(2018\)](#).
- [35] A. Celi, P. Massignan, J. Ruseckas, N. Goldman, I. B. Spielman, G. Juzeliunas, and M. Lewenstein, [Phys. Rev. Lett. **112**, 043001 \(2014\)](#).
- [36] N. Goldman, J. C. Budich, and P. Zoller, [Nat. Phys. **12**, 639 \(2016\)](#).
- [37] C. Qin, B. Wang, H. Long, K. Wang, and P. Lu, [J. Lightwave Technol. **34**, 3877 \(2016\)](#).
- [38] K. Fang, J. Luo, A. Metelmann, M. H. Matheny, F. Marquardt, A. A. Clerk, and O. Painter, [Nat. Phys. **14**, 465 \(2017\)](#).
- [39] D. L. Sounas and A. Alù, [Nat. Photonics **11**, 774 \(2017\)](#).
- [40] S. Ke, D. Zhao, Q. Liu, S. Wu, B. Wang, and P. Lu, [J. Lightwave Technol. **36**, 2510 \(2018\)](#).
- [41] M. C. Rechtsman, J. M. Zeuner, Y. Plotnik, Y. Lumer, D. Podolsky, F. Dreisow, S. Nolte, M. Segev, and A. Szameit, [Nature \(London\) **496**, 196 \(2013\)](#).
- [42] Q. Lin and S. Fan, [Phys. Rev. X **4**, 031031 \(2014\)](#).
- [43] K. Fang and S. Fan, [Phys. Rev. Lett. **111**, 203901 \(2013\)](#).
- [44] Y. J. Lin, R. L. Compton, K. Jiménez-García, W. D. Phillips, J. V. Porto, and I. B. Spielman, [Nat. Phys. **7**, 531 \(2011\)](#).
- [45] T. Oka and H. Aoki, [Phys. Rev. B **79**, 081406 \(2009\)](#).
- [46] H. Murata, A. Morimoto, T. Kobayashi, and S. Yamamoto, [IEEE J. Sel. Top. Quant. Elec. **6**, 1325 \(2000\)](#).

- [47] H. Lira, Z. Yu, S. Fan, and M. Lipson, [Phys. Rev. Lett. **109**, 033901 \(2012\)](#).
- [48] J. B. Pendry, [Phys. Rev. Lett. **85**, 3966 \(2000\)](#).
- [49] T. Xu, A. Agrawal, M. Abashin, K. J. Chau, and H. J. Lezec, [Nature \(London\) **497**, 470 \(2013\)](#).
- [50] T. Pertsch, T. Zentgraf, U. Peschel, A. Bräuer, and F. Lederer, [Phys. Rev. Lett. **88**, 093901 \(2002\)](#).
- [51] D. N. Christodoulides, F. Lederer, and Y. Silberberg, [Nature \(London\) **424**, 817 \(2003\)](#).
- [52] B. Wang, X. Zhang, F. J. García-Vidal, X. Yuan, and J. Teng, [Phys. Rev. Lett. **109**, 073901 \(2012\)](#).

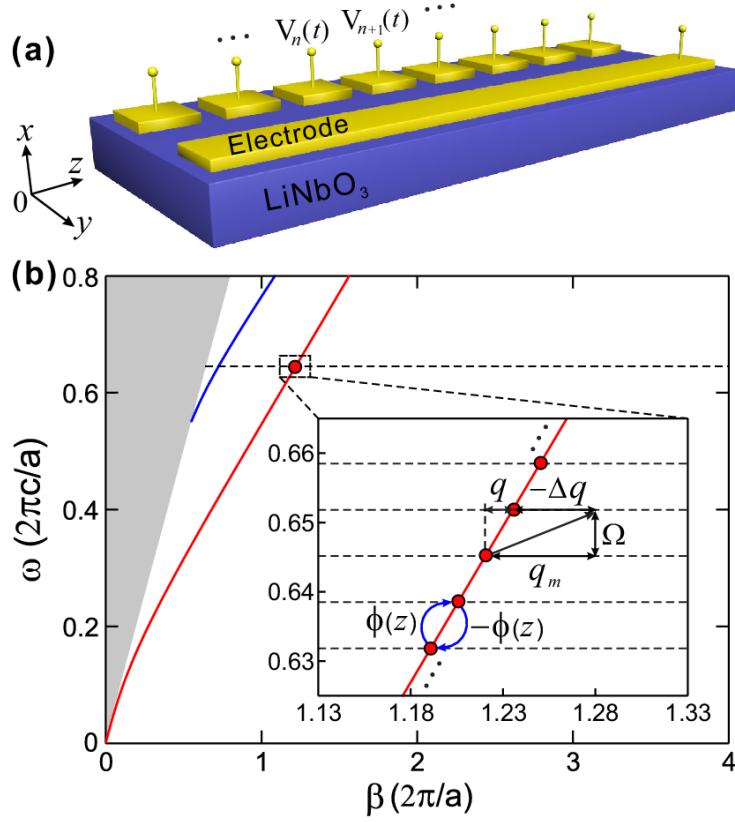


FIG. 1. (a) Schematic diagram of the waveguide modulator with periodic electrodes. The substrate is constituted with a LiNbO_3 slab waveguide with thickness $d = 0.5 \mu\text{m}$, background dielectric constant $\epsilon_d = 4.58$ ($n_0 = 2.14$) and dielectric modulation amplitude $\Delta\epsilon = 5 \times 10^{-3}$. (b) Photonic intraband transitions in TE_0 band (blue curved arrows). The red and blue curves represent TE_0 and TE_1 bands with the gray region denoting the light cone. Both frequencies and wavenumbers are normalized with respect to $a = 1 \mu\text{m}$. We choose $\omega_0/(2\pi c/a) = 0.6451$ ($\lambda_0 = 1.55 \mu\text{m}$) and $\Omega/2\pi = 20 \text{ GHz}$. $\Delta q = q - q_m$ is the wave vector mismatch with q_m and q being the modulation wavenumber and wavenumber difference between adjacent order modes. $\pm\phi(z)$ is the z -dependent, nonreciprocal phase shift accompanying photonic transitions.

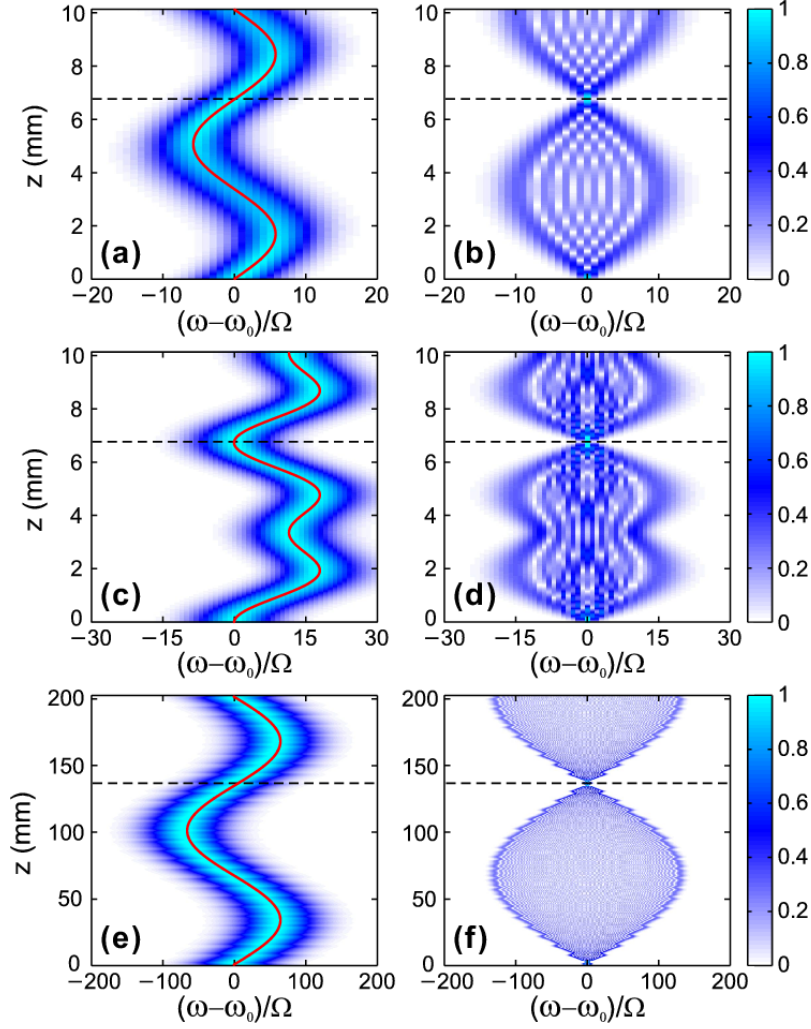


FIG. 2. (a) (b) Spectral evolutions of frequency BOs for a frequency comb (a) and a single frequency (b) input. The width of Gaussian envelope is $W = 5\Omega$. The modulation length is $L = 3Z_B/2$ with black dashed lines denoting $z = Z_B$. The modulation phase with respect to the initial Bloch momentum is $\phi - \phi_0 = \pi/2$. (c) (d) Spectral evolutions of frequency ABOs for a frequency comb (c) and a single frequency (d) input. The parameters are $W = 8\Omega$, $C_1 = C_2$ and $\phi_1 - \phi_0 = \phi_2 - \phi_0 = \pi$. (e) (f) Spectral evolutions of frequency SBOs for a frequency comb (e) and a single frequency (f) input. We choose $W = 50\Omega$, $\Delta\phi_m = \pi/2$, $\phi - \phi_0 = \phi_m - \phi_0 = 0$. The wave vector of ac force is $Q_m = \Delta q - m\Delta Q$ with $m = 1$ and $\Delta Q = \Delta q/20$, thus we have $Z_{SB} = 20Z_B$. The modulation length is $L = 3Z_{SB}/2$ and the black dashed lines denote $z = Z_{SB}$. The red solid lines denote the theoretical trajectories.

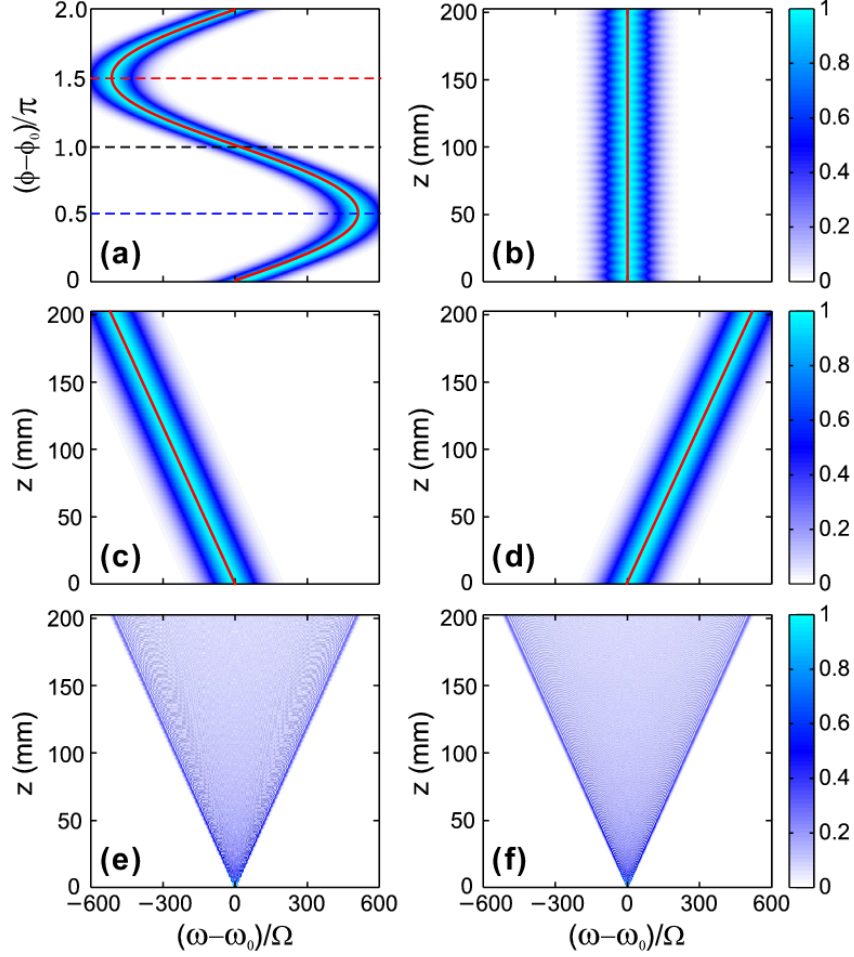


FIG. 3. (a) Output spectral evolution under a frequency comb input as $\phi - \phi_0$ varies from 0 to 2π as $L = 3Z_{\text{SB}}/2$. We choose $W = 100\Omega$, $Q_m = \Delta q - m\Delta Q$ with $m = 1$ and $\Delta Q = \Delta q/20$ such that $Z_{\text{SB}} = 20Z_{\text{B}}$. The blue, red and black dashed lines denote $\phi - \phi_0 = \pi/2$, $3\pi/2$ and π , respectively. (b)-(d) Spectral evolutions for a frequency comb input with $\phi - \phi_0 = 0$, $3\pi/2$, and $\pi/2$, respectively. The red solid lines denote the respective theoretical trajectories. (e) (f) The original and equivalent amplitude spectral evolutions under a single frequency input. The red solid lines denote the theoretical results.

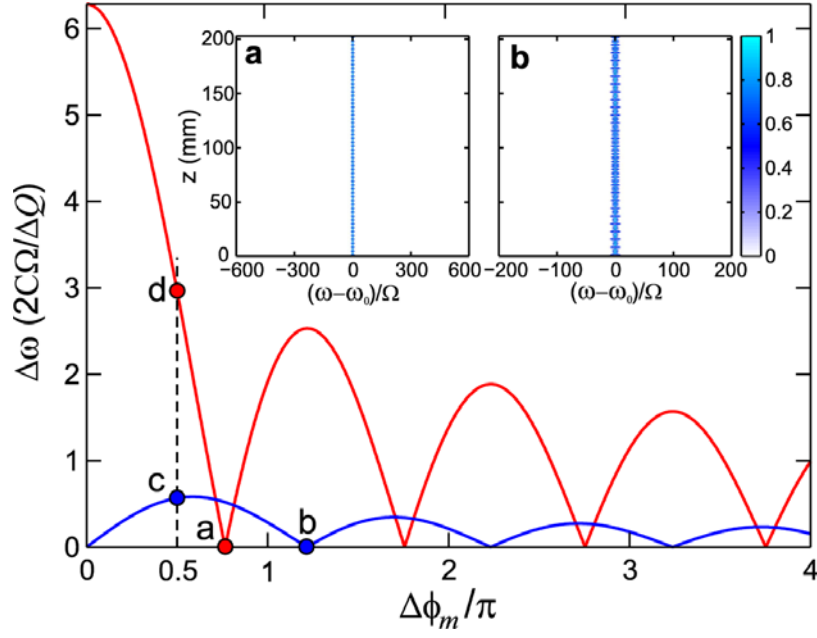


FIG. 4. The maximum frequency shift $\Delta\omega$ versus $\Delta\phi_m$ for both frequency directional shift (red) and SBOs (blue), respectively. We choose $L = Z_{SB}$ with other parameters kept the same with those in FIG. 2. Inserted a, spectral evolution for frequency directional shift under a single frequency input as $\Delta\phi_m = 2.40483$ (red circle a). Inserted b, spectral evolution for frequency SBOs as $\Delta\phi_m = 3.83171$ (blue circle b). The blue circle c and red circle d denote $\Delta\phi_m = \pi/2$, which represent the cases in FIG. 2 and FIG. 3, respectively.

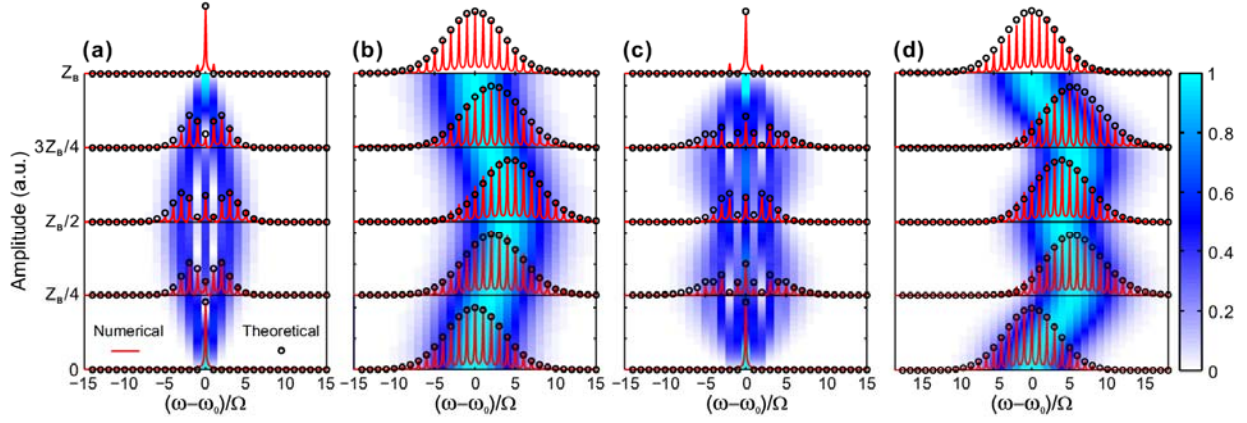


Fig. 5. (a) (b) Theoretical and numerical spectral evolutions of frequency BOs for a single frequency and a frequency comb input. Here we choose $\Omega/2\pi = 4$ THz, $\Delta\varepsilon = 0.5$ with other parameters kept the same with those in Fig. 2. (c) Theoretical and numerical spectral evolutions of frequency ABOs under a single frequency and a frequency comb input. The red dashed lines and black circles represent the numerical and theoretical spectra at $z = 0, Z_B/4, Z_B/2, 3Z_B/4$ and Z_B , which are obtained by first-principle simulations using COMSOL and by solving the coupled-mode equation of Eq. (1).

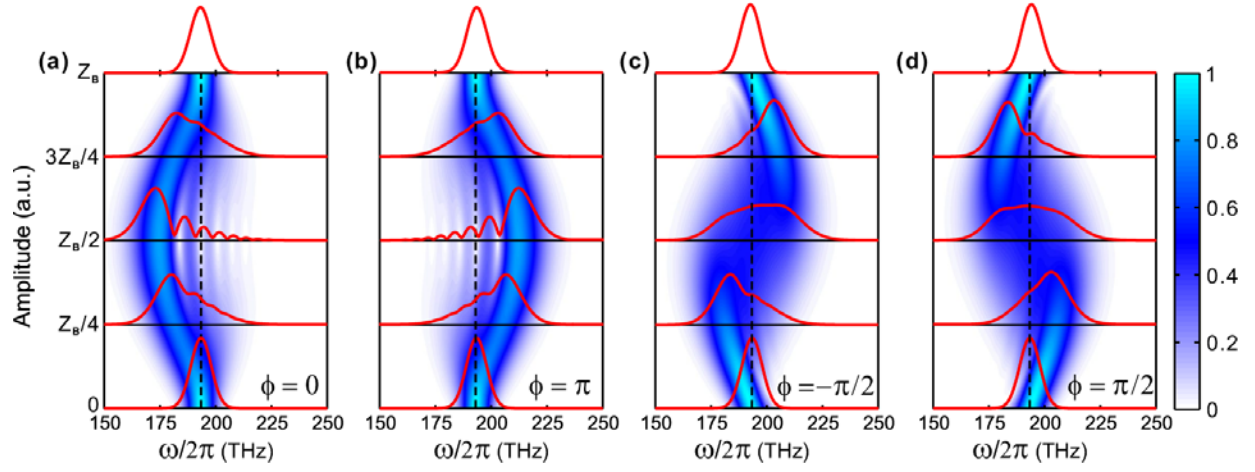


Fig. 6. Theoretical and numerical spectral evolutions of frequency BOs under an single ultra-short pulse input. We choose $\omega_0/2\pi = 193.4$ THz ($\lambda_0 = 1.55$ μm), $t_0 = 50$ ps and $\Delta t = 50$ fs, and thus the Gaussian spectral width is $\Delta\omega/2\pi = 40$ THz. The modulation phase with respect to the pulse arrival time is $\phi = 0, \pi, -\pi/2, \pi/2$ in (a) (b) (c) and (d), respectively. The red solid lines denote the numerical spectra distribution at $z = 0, Z_B/4, Z_B/2, 3Z_B/4$, which are obtained by using COMSOL Multiphysics.